Eur Biophys J (2008) 37:223–228
DOI 10.1007/s00249-007-0197-4

BIOPHYSICS LETTER

Intracellular heating of living cells through Néel relaxation of magnetic nanoparticles

Jean-Paul Fortin · Florence Gazeau · Claire Wilhelm

Received: 17 January 2007 / Revised: 23 May 2007 / Accepted: 28 May 2007 / Published online: 20 July 2007

Abstract Maghemite and cobalt ferrite anionic magnetic nanoparticles enter tumor cells and can be used as heat sources when exposed to a high-frequency magnetic field. Comparative studies of the two particles enable to unravel the magnetic heating mechanisms (Néel relaxation vs. Brown relaxation) responsible for the cellular temperature rise, and also to establish a simple model, adjusted to the experimental results, allowing to predict the intracellular heating efficiency of iron oxide nanoparticles. Hence, we are able to derive the best nanoparticle design for a given material with a view to intracellular hyperthermia-based applications.

Introduction

Magnetic nanoparticles are at the leading edge of biomedical colloid applications (Whitesides 2003). Indeed, these multifunctional agents can be used (1) for cellular labeling (Hogemann et al. 2002; Wilhelm et al. 2002b; Zhang et al. 2002), as they are much smaller than a living cell, (2) for bioseparation (Thiel et al. 1998) and drug targeting (Alexiou et al. 2006; Fortin-Ripoche et al. 2006; Hafeli 2004) on exposure to a magnetic force, (3) as contrast agents for magnetic resonance imaging (MRI) (Billotey et al. 2003; Bulte et al. 1999; Dodd et al. 1999), thanks to the local magnetic field they generate, and (4) as heat generators (for cancer therapy for example) (Jordan et al. 1999a; Moroz et al. 2002).

J.-P. Fortin · F. Gazeau · C. Wilhelm (✉)
Laboratoire Matière et Systèmes Complexes,
CNRS UMR 7057, Université Paris 7, Paris, France
e-mail: claire.wilhelm@univ-paris-diderot.fr

When exposed to a high-frequency magnetic field, magnetic monodomain nanoparticles generate heat through oscillation of their magnetic moment (Jordan et al. 1993). Dissipation can be due to rotation of the entire magnetic particle within a surrounding liquid (Brownian relaxation) and/or to rotation of the magnetic moment within the magnetic core (Néel relaxation). Generally, heating power is dominated by the faster regime of relaxation. However, it is not easy to distinguish between the contributions of the Brown and Néel mechanisms, and few studies have focused on mechanisms by which iron oxide nanoparticles generate heat (Hergt et al. 2004; Jordan et al. 1993; Rosensweig 2002; Wang et al. 2005).

In recent years, local heat generation has been tested as a means of destroying malignant tumors. Direct injection of magnetic nanoparticles into solid tumors, followed by exposure to an alternating magnetic field, has been shown to be capable of inducing tumor regression (Hilger et al. 2001; Ito et al. 2003; Jordan et al. 1997). The challenge is now to design magnetic nanoparticles capable of penetrating selectively into cancer cells in order to generate lethal heating from the cell inside (Ito et al. 2005; Jordan et al. 1999b). In this study we tested anionic nanoparticles of two different iron oxides for their capacity to be internalized by malignant cells and to generate heat intracellularly. The two particle types show the same excellent intracellular labeling efficiency, thanks to their nanoscale dimensions and similar surface charges. We examined whether the mechanisms and efficiency of heat generation by these magnetic mediators were modified following their internalization, by comparing the heating power of the two nanoparticles when dispersed in various carrier fluids and after cellular uptake and we modeled heat generation by a variety of particle designs.

The two nanoparticles types used, both synthesized with Massart's method (Massart 1981), are composed of maghemite (γFe_2O_3) or cobalt ferrite ($CoFe_2O_4$). The ionic precursor is obtained by coprecipitation of iron chloride salts for maghemite nanoparticles, together with cobalt chloride salts for cobalt ferrite ones. Nanoparticles are then chelated with citric acid which confers to the nanoparticles negative surface charges due to the carboxylate groups and ensure colloidal stability in aqueous suspension through electrostatic repulsion. Their size distributions are deduced from the fit of their magnetization curves and are well described by a log-normal distribution of particle diameter d, $P(d) = \frac{1}{\sqrt{2\pi}\sigma d}\exp\left[-\frac{\ln^2(d/d_0)}{2\sigma^2}\right]$ with a characteristic diameter d_0 and polydispersity index σ. The maghemite and cobalt ferrite nanoparticles had d_0 values of 7.45 and 9.7 nm, respectively, and σ values of 0.35 for both. These particles are well suited to unravell the relative contributions of the two mechanisms of magnetically induced heating. Indeed, maghemite and cobalt ferrite nanoparticles differ essentially by their magnetic anisotropy energy E_A ($E_A = KV$, where K is the anisotropy constant ($K = 1.6 \times 10^4$ J m^{-3} for maghemite, $K = 1.23 \times 10^5$ J m^{-3} for cobalt ferrite (Fortin et al. 2007)) and V is the magnetic core volume), meaning that they generate heat through different mechanisms (see below).

Tumor cells efficiently internalize both maghemite and cobalt ferrite anionic nanoparticles

Both nanoparticle types entered tumor cells with similar efficiency and followed the same intracellular pathway. Human prostatic adenocarcinoma cells (PC3) were cultured in complete DMEM culture medium. They were magnetically labeled by adding filter-sterilized suspension of magnetic nanoparticles in serum-free culture medium at an iron mass concentration [Fe] = 2.5 g l^{-1} at 37°C for 15 min to 2 h. Using magnetophoresis (Wilhelm et al. 2002a), an original quantitative magnetic assay, we measured the cellular uptake of both particle types as a function of the incubation time. Briefly, in this assay method, magnetic cells dispersed in culture medium are exposed to a constant magnetic field gradient. Their velocity along the gradient results from the equilibrium between the magnetic force and resistance by viscous forces. This velocity directly yields the cell magnetization, which is equivalent to the amount of particles in the cell. Velocity measurements of 400 independent cells were used to obtain the whole cellular uptake distribution and mean value. The uptake curves (Fig. 1a, b) show that the cobalt ferrite and maghemite nanoparticles had similar efficient and saturable cellular uptake, owing to their similar sizes

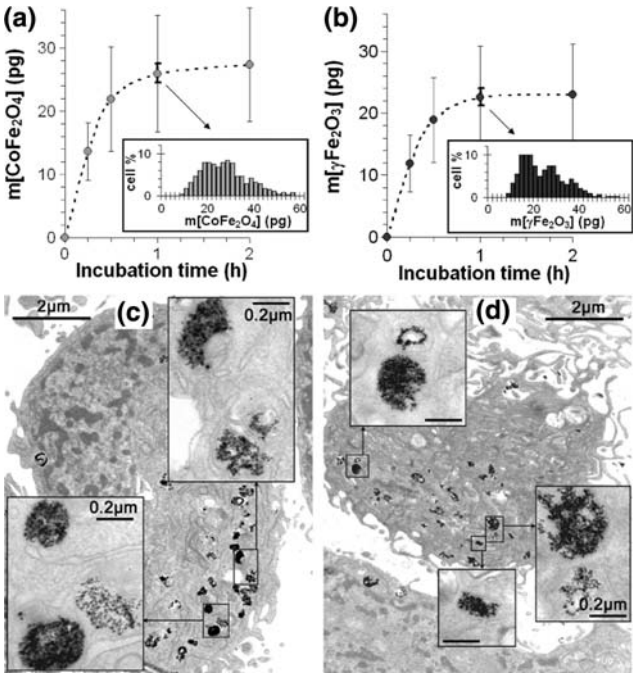

Fig. 1 Intracellular magnetic labeling of PC3 tumor cells. (**a, b**) Uptake curves for cobalt ferrite nanoparticles (**a,** *bottom*) and maghemite (**b,** *bottom*) by PC3 tumor cells as a function of incubation time with [Fe] = 2.5 g l^{-1} in the culture medium. *Bars* represent the deviation for the cell population from the mean value (between-cell differences in endocytotic capacity). The corresponding distribution for the 1 h incubation condition is shown in the inset of each part. The error from one preparation to another is shown as a *bold bar* on the 1 h uptake curve and was below 5%. (**c, d**) Electron micrographs of PC3 cells incubated with cobalt ferrite (**c**) and maghemite (**d**) nanoparticles (1 h, [Fe] = 2.5 g l^{-1}). The particles are electron-dense and appear as *black points* on the images. They are packed within intracellular vesicles. Note that the extracellular space is free of nanoparticles

and to their negative charges, which create cell membrane affinity (Wilhelm et al. 2002b). For intracellular hyperthermia experiments, cells were incubated with the particles for 1h at an iron mass concentration of 2.5 g l^{-1}. In these conditions, mean cellular uptake mass was 22.6 pg of maghemite per cell (equivalent iron mass m_{Fe} = 15.8 pg cell^{-1}) and 25.9 pg of cobalt ferrite per cell (m_{Fe} = 12.4 pg cell^{-1}). Observations with transmission electron microscopy showed that both nanoparticles types are confined intracellularly inside 0.5 µm-diameters membrane-bound vesicles known as endosomes (Fig. 1c, d) (Wilhelm et al. 2003). It has been shown that nanoparticle confinement in endosomes reduces MRI relaxivities, probably through saturation of the relaxing effect of particles concentrated within endosomes (Billotey et al. 2003). By contrast, the consequences of this intracellular confinement on the particles' magnetic heating properties are not known.

Intracellular magnetic nanoheaters warm tumor cells up to 45°C

For intracellular hyperthermia experiments, 20 million labeled cells were dispersed in 0.3 ml of complete culture medium in a 0.5-ml vial. Magnetic hyperthermia was achieved by applying an alternating magnetic field. The sample was inserted in a copper coil (diameter 16 mm), cooled with thermostating liquid (nonane), which produces an alternating magnetic field in the frequency range of 300 kHz–1.1 MHz and with an amplitude up to 31 mT. The sample volume (0.3 ml) was chosen to minimize the effects of magnetic field inhomogeneities. The nonane temperature was tuned in order to obtain an equilibrium temperature of 37°C for each amplitude and each frequency of the applied magnetic field. Temperature was measured with a fluorooptic probe (Luxtron Corp. fiber thermometer). Figure 2a shows temperature elevation in the cell suspensions with increasing amounts of magnetic cells, during the application of the magnetic field (700 kHz, 31 mT). The temperature gradient diminished as the fraction of labeled cells in the pellet decreased.

Intracellular magnetic heating is less efficient than magnetic fluid heating in the thermal sense

To evaluate the effect of intracellular confinement on heating potency, we compared the steady-state temperature reached inside the pellet after 10 min of magnetic field exposure, and the initial linear rise in temperature versus time dependence, between intracellular and free nanoparticles. The plateau temperature was lower with intracellular maghemite nanoparticles than with the same nanoparticles dispersed in water (magnetic fluid) at an equivalent concentration (Fig. 2b). This plateau temperature is dependent on the maghemite concentration in the pellet (0.3, 1.2 and 1.5 g l^{-1}) and on the geometry of the pellet (owing to heat transfer to the tube walls). In contrast, the initial linear rise in temperature is independent of the sample geometry and was used to derive the specific loss power (SLP), defined as the amount of energy converted into heat per time and per mass of magnetic material: $\mathrm{SLP} = \frac{CV_s}{m}\frac{dT}{dt}$, where C is the volumetric specific heat capacity of the sample (C_{water} = 4185 JL^{-1} K^{-1}, $C_{glycerol}$ = 3086 JL^{-1} K^{-1}), V_s is the sample volume (0.3 ml) and m is the mass of magnetic material in the sample. Figure 2c, d compare experimental SLP values as a function of the magnetic field frequency, with maghemite and cobalt ferrite nanoparticles, respectively, dispersed in water or glycerol, and for the same nanoparticles internalized by cells (with surrounding considered to be water in endosomes). Maghemite particles had an SLP of 203 W g^{-1} at 700 kHz when dispersed in water, and

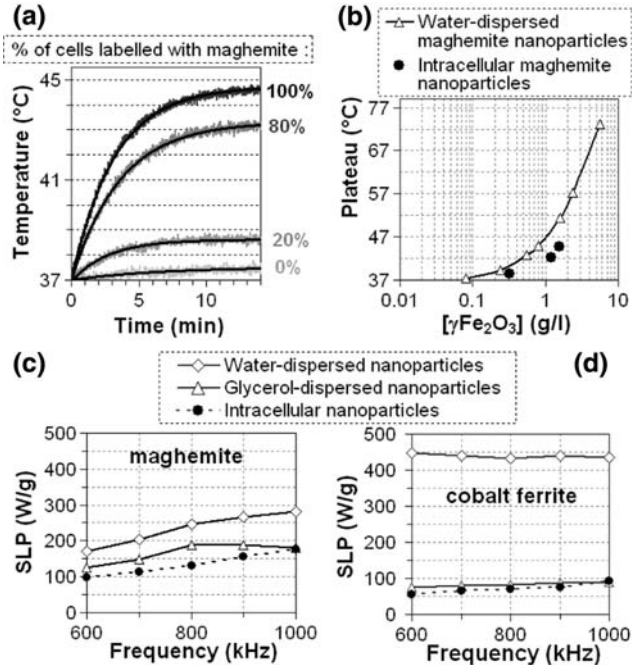

Fig. 2 **a** Heating of cells containing maghemite nanoparticles. Pellets with a volume of 300 µl and containing 20 million cells were used. Temperature was recorded every 0.7 s after switching on the power supply. The higher the proportion of magnetically labeled cells (0, 20, 80, 100%), the more the pellet heated, reaching a temperature of 44.6°C with maghemite-labeled cells alone (no unlabeled cells). **b** Comparison of the maximum temperature reached with maghemite nanoparticles dispersed in water and within cells, as a function of the iron concentration. **c, d** Specific loss power (SLP) for maghemite (**c**) and cobalt ferrite (**d**) nanoparticles dispersed in water or glycerol or packed inside intracellular vesicles, as a function of the frequency of the AC magnetic field (31 mT). Nanoparticles dispersed in glycerol and nanoparticles packed inside intracellular vesicles had lower SLPs than the nanoparticles dispersed in water. The difference was much more pronounced with cobalt ferrite than with maghemite

148 W g^{-1} when dispersed in glycerol (Fig. 2c). When dispersed in water, cobalt ferrite particles had high SLP values (440 W g^{-1} at 700 kHz, 31 mT) but these diminished drastically as the solvent viscosity increased (79 W g^{-1} in glycerol) (Fig. 2d). Thus, the increase in carrier fluid viscosity, which prolongs Brownian relaxation, had a more pronounced effect on cobalt ferrite particles than on maghemite particles. When the nanoparticles were confined inside intracellular vesicles, similar reductions in SLP values were observed relative to aqueous suspensions: heating was therefore less efficient when the particles, and especially cobalt ferrite particles, were internalized in cells.

Intracellular magnetic nanoparticles generate heat through Néel relaxation

Figures 3, 4, 5 compare our experimental results and theoretical predictions. Analytical relationships of power

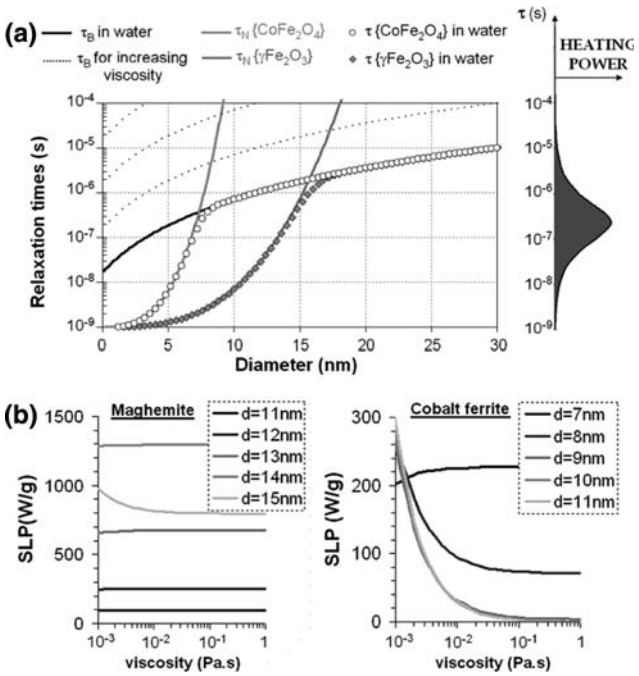

Fig. 3 **a** Characteristic times of magnetic moment orientational dynamics as a function of particle diameter. The Brownian relaxation time is identical for maghemite and cobalt ferrite nanoparticle of given diameter d as it depends only on the particle geometry and on the viscosity of the surrounding medium. It is presented both for particles dispersed in water (viscosity 7×10^{-3} Pa × s at 37°C) or in carrier media of viscosity 10, 100 and 1000 times the water value (*dotted lines*). The Néel relaxation time varies exponentially with magnetic anisotropy energy and is much higher for cobalt ferrite particles (high magnetic anisotropy) than for maghemite particles (low magnetic anisotropy). The effective relaxation time τ (roughly the shortest time) is represented as *dotted circles* for maghemite and cobalt ferrite in water. The heating efficiency is shown on the *right* as a function of the effective relaxation time τ. **b** Calculated SLP (31 mT; 700 kHz) for monodispersed particles of maghemite (*left*) and cobalt ferrite (*right*) as a function of the viscosity of carrier fluid. The maghemite SLP is independent of viscosity for particles below 14 nm and slightly falls with viscosity for larger diameters. In contrast, the SLP of cobalt ferrite particles with diameters above 8 nm collapses with increasing viscosity, due to the abrogation of the Brownian contribution. Above viscosities 100 times that of water, the SLP no longer changes, being exclusively due to Néel relaxation

dissipation by a magnetic nanoparticle of given diameter d can be derived as

$$SLP(d) = \frac{\mu_0 \chi_0 H_0^2}{2\rho\phi}\omega\frac{\omega\tau(d)}{1+\{\omega\tau(d)\}^2} \quad (1)$$

(Rosensweig 2002), where χ_0 is the static susceptibility of the suspension (proportional to the volume fraction of particles φ), ρ the mass per unit volume of iron oxide, ω the magnetic field frequency and τ the effective relaxation time defined as $1/\tau = 1/\tau_N + 1/\tau_B$. The Néel relaxation time τ_N varies exponentially with anisotropy energy E_A: $\tau_N = \tau_0 \exp E_A/k_bT$ where $\tau_o = 10^{-9}$s, T is the absolute

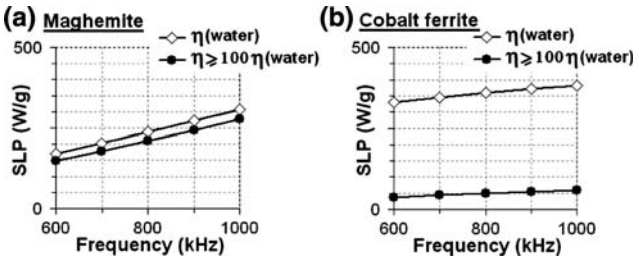

Fig. 4 Calculated SLPs of maghemite (**a**) and cobalt ferrite nanoparticles (**b**) used in this study, as a function of the frequency of the AC magnetic field (31 mT). *White diamonds* were calculated for water viscosity and closely fit the experimental points for nanoparticles dispersed in water (Fig. 2c, d). *Black circles* were calculated by assuming Brownian relaxation times (medium effective viscosity) at least 100-fold longer than that observed in water. Note that these theoretical values closely match the experimental points obtained for intracellular nanoparticles (Fig. 2c, d)

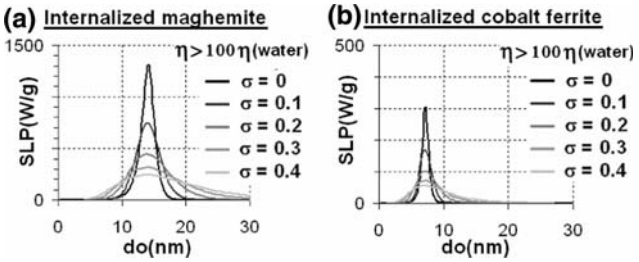

Fig. 5 Predicted SLPs of polydispersed maghemite (**a**) and ferrite cobalt (**b**) nanoparticles internalized by the cells, as a function of their characteristic diameter d_0 and polydispersity index σ

temperature and k_b the Boltzmann constant. The Brownian relaxation time τ_B depends on both the carrier fluid viscosity η and on the hydrodynamic volume V_H of the particle: $\tau_B = 3\eta V_H/kT$. The shorter relaxation time determines which relaxation mechanism predominates. The calculated Brown and Néel relaxation times, together with the effective time τ, are shown in Fig. 3a as a function of the particle diameter d for both magnetic materials. For nanoparticles dispersed in water, in the diameter range 8–15 nm, Brownian relaxation predominates with cobalt ferrite and Néel relaxation with maghemite nanoparticles. Heating efficiency varies as $\omega^2\tau/(1+\omega^2\tau^2)$ and is superimposed on the figure with respect to the effective time τ, for a frequency of 700 kHz. It appears that heating is efficient for relaxation times approximately between 5×10^{-9} and 10^{-5} s. For particles larger than 5 nm diameter, the upper limit of 10^{-5} s is attained by the Brownian relaxation time if viscosity exceeds that of water by 100-fold, the Brownian contribution to heating is therefore abrogated. The subsequent calculated SLPs (at 700 kHz and 31 mT) are shown in Fig. 3b for monodisperse ($\sigma = 0$) nanoparticles of maghemite and cobalt ferrite of different diameters d, as a function of the media viscosity. The SLP

for maghemite particles is the largest with nanoparticles of about 14 nm in diameter and is mostly due to Néel relaxation (i.e. viscosity-independent), whereas the SLP for cobalt ferrite particles is large, 7–8 nm diameter, and is mainly due to Brownian relaxation with particles above 8 nm in diameter (highly sensitive to viscosity).

Before using this model to predict experimental SLPs with polydispersed preparations, one must integrate the monodisperse calculated SLP (Eq. 1) with respect to the log-normal size distribution (given by both characteristic diameter d_o and polydispersity index σ). Figure 4a, b represents the calculated SLP values for maghemite (d_o = 7.45 nm; σ = 0.35) and cobalt ferrite (d_o = 9.7 mn; σ = 0.35), respectively, as a function of the AC field frequency (field magnitude 31 mT). For nanoparticles dispersed in water, the calculated SLPs closely match the measured values (Fig. 2c, d). The predicted SLP values, calculated with no Brownian contribution to heating (medium viscosity 100 times and more that of water), again closely matched the measured values for intracellular nanoparticles (compare Figs. 4a and 2c for maghemite and Figs. 4b and 2d for cobalt ferrite). The increase in effective viscosity for nanoparticles concentrated within intracellular vesicles is probably related to the impairment of Brownian motion by local viscous forces, as well as magnetic interparticle interactions and steric interactions. The important point is that intracellular confinement of the nanoparticles abrogates the Brownian contribution to heating. In other words, intracellular hyperthermia mostly originates from Néel relaxation.

These results allow us to design new magnetic nanoparticles for more efficient intracellular hyperthermia. Figure 5a, b shows the predicted SLPs for intracellular maghemite and cobalt ferrite nanoparticles with different polydispersity values (σ = 0–0.4), as a function of the characteristic diameter *d*o of the particles distribution. The highest SLP values obtained with cobalt ferrite nanoparticles are lower more than three times than those obtained with maghemite nanoparticles. However, for particles with a diameter below 10 nm, cobalt ferrite is still more suitable for intracellular hyperthermia than maghemite. The optimal particle design corresponds to monodispersed 7.3-nm cobalt ferrite nanoparticles, which yield an SLP of 295 W g^{-1} at 700 kHz and 31 mT. For diameters above 10 nm, the SLP starts to increase with maghemite nanoparticles and reaches its highest value of 1280 W g^{-1} (700 kHz, 31 mT) for monodispersed nanoparticles 14.3 nm in diameter. Such maghemite nanoparticles would be the best candidates for intracellular applications, as they would generate ten times more heat than the particles used here.

To conclude, we describe two types of magnetic nanoheaters that generate magnetic energy through different mechanisms (principally Brown relaxation with cobalt ferrite and Néel relaxation with maghemite). They enter cells with similar efficiency, thanks to their similar nanoscopic design (size and ionic stabilization), and follow the same intracellular pathway. At equivalent magnetic material concentrations, intracellular nanoparticles generated less heat than the same nanoparticles dispersed in water. This difference was attributed to the abrogation of the Brownian contribution to heat generation when the particles were confined within intracellular vesicles, implying that intracellular magnetic nanoparticles generate heat exclusively through the Neel phenomenon. In the same manner, the heating of non-internalized particles in tissues will strongly depend on their coupling with the extracellular matrix. These findings pave the way for an efficient intracellular nanotool that could be used to heat selected targets "at a distance". Magnetic nanoheaters previously used for direct injection into tumors in vivo had SLPs comprised between 40 and 200 W g^{-1}, depending on the magnetic field magnitude and frequency. The maghemite anionic nanoparticles tested here (SLP 203 W g^{-1} at 700 kHz and 31 mT), and especially the cobalt ferrite nanoparticles (SLP 440 W g^{-1} at 700 kHz and 31 mT), are therefore good candidates for direct in vivo injection. To perform targeted intracellular hyperthermia in vivo, the concentration at the target site will be critical. As molecular targeting will be one of the main difficulties, individual nanoparticle heating efficiency will be crucial. By unravelling the mechanisms of intracellular heating, we show that nanoparticle design can be optimized to maximize heating potency through the Néel mechanism. Maghemite nanoparticles with a monodispersed diameter of 14 nm could improve heating efficiency by a factor of more than ten, thereby diminishing by the same factor the amount of nanoparticles that have to be delivered intracellularly. The challenge is now to specifically address these nanoparticles to tumor tissues after intravenous administration. Tumor-specific magnetic nanoparticles (DeNardo et al. 2005; Ito et al. 2004; Montet et al. 2006; Sun et al. 2006) are currently being developed for both diagnostic and therapeutic purposes. Combining particles addressing in vivo with high intracellular heating performance is full of promises for future cancer treatments.

Acknowledgments We thank Jean-Claude Bacri for fruitful discussions, Christine Ménager and Sophie Neveu for providing us with the nanoparticles, Christine Longin and Sophie Chat for assistance in electron microscopy and Jacques Servais for technical help. This work was supported by ACI n°145 NANOSCIENCE of the French Ministry of research.

References

Alexiou C, Schmid RJ, Jurgons R, Kremer M, Wanner G, Bergemann C, Huenges E, Nawroth T, Arnold W, Parak FG (2006) Targeting

cancer cells: magnetic nanoparticles as drug carriers. Eur Biophys J 35:446–450

Billotey C, Wilhelm C, Devaud M, Bacri JC, Bittoun J, Gazeau F (2003) Cell internalization of anionic maghemite nanoparticles: quantitative effect on magnetic resonance imaging. Magn Reson Med 49:646–654

Bulte JW, Zhang S, van Gelderen P, Herynek V, Jordan EK, Duncan ID, Frank JA (1999) Neurotransplantation of magnetically labeled oligodendrocyte progenitors: magnetic resonance tracking of cell migration and myelination. Proc Natl Acad Sci USA 96:15256–15261

DeNardo SJ, DeNardo GL, Miers LA, Natarajan A, Foreman AR, Gruettner C, Adamson GN, Ivkov R (2005) Development of tumor targeting bioprobes ((111)In-chimeric L6 monoclonal antibody nanoparticles) for alternating magnetic field cancer therapy. Clin Cancer Res 11:7087s–7092s

Dodd SJ, Williams M, Suhan JP, Williams DS, Koretsky AP, Ho C (1999) Detection of single mammalian cells by high-resolution magnetic resonance imaging. Biophys J 76:103–109

Fortin-Ripoche JP, Martina MS, Gazeau F, Menager C, Wilhelm C, Bacri JC, Lesieur S, Clement O (2006) Magnetic targeting of magnetoliposomes to solid tumors with MR imaging monitoring in mice: feasibility. Radiology 239:415–424

Fortin JP, Wilhelm C, Servais J, Ménager C, Bacri JC, Gazeau F (2007) Size-sorted anionic iron oxide nanomagnets as colloidal mediators for magnetic hyperthermia. JACS 129:2628–2635

Hafeli UO (2004) Magnetically modulated therapeutic systems. Int J Pharm 277:19–24

Hergt R, Hiergeist R, Hilger I, Kaiser WA, Lapatnikov Y, Margel S, Richter U (2004) Maghemite nanoparticles with very high AC-losses for application in RF-magnetic hyperthermia. J Magn Magn Mater 270:345–357

Hilger I, Andra W, Hergt R, Hiergeist R, Schubert H, Kaiser WA (2001) Electromagnetic heating of breast tumors in interventional radiology: in vitro and in vivo studies in human cadavers and mice. Radiology 218:570–575

Hogemann D, Ntziachristos V, Josephson L, Weissleder R (2002) High throughput magnetic resonance imaging for evaluating targeted nanoparticle probes. Bioconjug Chem 13:116–121

Ito A, Tanaka K, Honda H, Abe S, Yamaguchi H, Kobayashi T (2003) Complete regression of mouse mammary carcinoma with a size greater than 15 mm by frequent repeated hyperthermia using magnetite nanoparticles. J Biosci Bioeng 96:364–369

Ito A, Shinkai M, Honda H, Kobayashi T (2005) Medical application of functionalized magnetic nanoparticles. J Biosci Bioeng 100:1–11

Ito A, Kuga Y, Honda H, Kikkawa H, Horiuchi A, Watanabe Y, Kobayashi T (2004) Magnetite nanoparticle-loaded anti-HER2 immunoliposomes for combination of antibody therapy with hyperthermia. Cancer Lett 212:167–175

Jordan A, Wust P, Fahling H, John W, Hinz A, Felix R (1993) Inductive heating of ferrimagnetic particles and magnetic fluids: physical evaluation of their potential for hyperthermia. Int J Hyperthermia 9:51–68

Jordan A, Scholz R, Wust P, Fahling H, Krause J, Wlodarczyk W, Sander B, Vogl T, Felix R (1997) Effects of magnetic fluid hyperthermia (MFH) on C3H mammary carcinoma in vivo. Int J Hyperthermia 13:587–605

Jordan A, Scholz R, Wust P, Fakhling R, Felix R (1999a) Magnetic fluid hyperthermia (MFH): cancer treatment with AC magnetic field induced excitation of biocompatible superparamagnetic nanoparticles. J Mag Mag Mat 201:413–419

Jordan A, Scholz R, Wust P, Schirra H, Schiestel T, Schmidt H, Felix R (1999b) Endocytosis of dextran and silan-coated magnetite nanoparticles and the effect of intracellular hyperthermia on human mammary carcinoma cells in vitro. J Mag Mag Mat 194:185–196

Massart R (1981) Preparation of aqueous magnetic liquids in alkaline and acidic media. IEEE Trans Magn 17:1247–1248

Montet X, Montet-Abou K, Reynolds F, Weissleder R, Josephson L (2006) Nanoparticle imaging of integrins on tumor cells. Neoplasia 8:214–222

Moroz P, Jones SK, Gray BN (2002) Magnetically mediated hyperthermia: current status and future directions. Int J Hyperthermia 18:267–84

Rosensweig RE (2002) Heating magnetic fluid with alternating magnetic field. J Magn Magn Mater 252:370–374

Sun EY, Josephson L, Kelly KA, Weissleder R (2006) Development of nanoparticle libraries for biosensing. Bioconjug Chem 17:109–113

Thiel A, Scheffold A, Radbruch A (1998) Immunomagnetic cell sorting–pushing the limits. Immunotechnology 4:89–96

Wang X, Gu H, Yang Z (2005) The heating effect of magnetic fluids in an alternating magnetic field. J Magn Magn Mater 293:334–340

Whitesides GM (2003) The 'right' size in nanobiotechnology. Nat Biotechnol 21:1161–1165

Wilhelm C, Gazeau F, Bacri JC (2002a) Magnetophoresis and ferromagnetic resonance of magnetically labeled cells. Eur Biophys J 31:118–125

Wilhelm C, Gazeau F, Roger J, Pons JN, Bacri JC (2002b) Interaction of anionic superparamagnetic nanoparticles with cells: kinetic analyses of membrane adsorption and subsequent internalization. Langmuir 18:8148–8155

Wilhelm C, Cebers A, Bacri JC, Gazeau F (2003) Deformation of intracellular endosomes under a magnetic field. Eur Biophys J 32:655–660

Zhang Y, Kohler N, Zhang M (2002) Surface modification of superparamagnetic magnetite nanoparticles and their intracellular uptake. Biomaterials 23:1553–1561